BNST neurocircuitry in humans

Suzanne N. Avery [a,b,1], Jacqueline A. Clauss [a,b,1], Danny G. Winder [a,c], Neil Woodward [a,b,d],
Stephan Heckers [a,b,d], Jennifer Urbano Blackford [a,b,d,e,*]

[a] Vanderbilt Brain Institute, Vanderbilt University, Nashville, TN 37232, USA
[b] Psychiatric Neuroimaging Program, Vanderbilt University School of Medicine, Nashville, TN 37212, USA
[c] Department of Molecular Physiology and Biophysics, Vanderbilt University School of Medicine, Nashville, TN 37232, USA
[d] Department of Psychiatry, Vanderbilt University School of Medicine, Nashville, TN 37212, USA
[e] Department of Psychology, Vanderbilt University School of Medicine, Nashville, TN 37240, USA

ABSTRACT

Anxiety and addiction disorders are two of the most common mental disorders in the United States, and are typically chronic, disabling, and comorbid. Emerging evidence suggests the bed nucleus of the stria terminalis (BNST) mediates both anxiety and addiction through connections with other brain regions, including the amygdala and nucleus accumbens. Although BNST structural connections have been identified in rodents and a limited number of structural connections have been verified in non-human primates, BNST connections have yet to be described in humans. Neuroimaging is a powerful tool for identifying structural and functional circuits in vivo. In this study, we examined BNST structural and functional connectivity in a large sample of humans. The BNST showed structural and functional connections with multiple subcortical regions, including limbic, thalamic, and basal ganglia structures, confirming structural findings in rodents. We describe two novel connections in the human brain that have not been previously reported in rodents or non-human primates, including a structural connection with the temporal pole, and a functional connection with the paracingulate gyrus. The findings of this study provide a map of the BNST's structural and functional connectivity across the brain in healthy humans. In large part, the BNST neurocircuitry in humans is similar to the findings from rodents and non-human primates; however, several connections are unique to humans. Future explorations of BNST neurocircuitry in anxiety and addiction disorders have the potential to reveal novel mechanisms underlying these disabling psychiatric illnesses.

© 2014 Elsevier Inc. All rights reserved.

Introduction

Elucidating the neural basis of common psychiatric disorders, such as anxiety and addiction, can guide the development of novel preventions and therapeutics. Complex states likely result from alterations in underlying neurocircuitry, and both structural and functional measures of connectivity show promise as disease biomarkers. Neuroimaging methods provide a powerful tool for examining neural circuits *in vivo* and progress has been made in identifying the neurocircuitry of anxiety (Shin and Liberzon, 2010) and addiction (Koob and Volkow, 2010). However, most investigations have focused on larger brain regions due to concerns about the ability of neuroimaging methods to measure smaller structures. With advances in imaging technology and analytic techniques, the exploration of circuits involving smaller brain regions is now possible.

A prime candidate for this type of investigation is the bed nucleus of the stria terminalis (BNST), a small structure in the basomedial forebrain. Research in rodents has established that the BNST mediates sustained anxiety responses (Davis et al., 1997; Hammack et al., 2004; Lungwitz et al., 2012; Sullivan et al., 2004; Waddell et al., 2006). Preliminary evidence also links BNST function to anxiety in non-human primates (Fox et al., 2008; Kalin et al., 2005) and humans (Alvarez et al., 2011; Grupe et al., 2013; Hasler et al., 2007; Somerville et al., 2010, 2013). BNST function also mediates reward-seeking and addictive behaviors in rodents (Dumont et al., 2005; Kash et al., 2008; Koob and Le Moal, 2008; Leri et al., 2002; Silberman and Winder, 2013) and humans (O'Daly et al., 2012).

Specific neural circuits—rather than specific brain regions—are crucial for complex behaviors, as recently demonstrated using optogenetics (Jennings et al., 2013; Kim et al., 2013). Most of our knowledge about BNST structural connectivity comes from tracer studies in rodents, which have shown that the BNST has extensive connections to other limbic regions—including the amygdala, hypothalamus, hippocampus, periaqueductal gray, and infralimbic cortex (Dong and Swanson, 2004a,b, 2006a,b,c; Dong et al., 2001b)—and striatal regions, including the nucleus accumbens and ventral tegmental area (Dong et al.,

2001b). In primates, however, surprisingly little is known about BNST neurocircuitry. Tract-tracing studies in non-human primates have focused predominantly on relationships between the BNST and other limbic structures (Price and Amaral, 1981). In a single study using functional connectivity in humans and non-human primates, Oler et al. (2012) demonstrated that the BNST is functionally connected with the central nucleus of the amygdala, consistent with previously demonstrated rodent and non-human primate anatomical connections (Dong et al., 2001a). The BNST is much larger and more developed in humans than in rodents (Lesur et al., 1989), suggesting that BNST circuits may be altered in humans; however, to our knowledge, no studies have examined BNST structural or functional connectivity across the whole human brain. In the present study, we used diffusion tensor imaging (DTI) and resting state functional MRI (rs-fMRI) methods to identify patterns of BNST structural and functional connectivity in humans.

Materials and methods

Participants

We selected 82 DTI scans and 99 rs-fMRI scans of healthy controls with no psychiatric illnesses from two ongoing studies for this analysis. Scans were selected based on the following criteria: 1) the participant had no current or past psychiatric disorders, as determined by the Structured Clinical Interview for the DSM-IV (SCID I-P) (First et al., 2002); 2) participants were not on any psychotropic medications (within the past 6 months); and 3) the scan was determined to have good data quality (see quality methods below). Sixty-one participants overlapped between the DTI and rs-fMRI analyses. Participants included in this analysis were 17–57 years old (mean ± SD = 30.6 ± 11.3 years), 47.7% female, and 84.7% right-handed. Participants represented a variety of ethnicities including Caucasian (66.9%), African-American (26.2%), Asian (5.4%), and other (1.5%). The Vanderbilt University Institutional Review Board approved the study and written informed consent was obtained from each participant.

BNST delineation

The BNST is a small (approximately 190 mm^3 in humans, compared to the amygdala at approximately 1800 mm^3) cluster of nuclei located in the basomedial forebrain. Due to the small size of the BNST and its close proximity to other subcortical gray matter nuclei (Lesur et al., 1989), the boundaries of the BNST are often difficult to delineate on standard T1-weighted (T1W) anatomical images. To overcome this challenge and accurately delineate the boundaries of the BNST in the human brain, we collected an ultra high-resolution anatomical image at 7 Tesla (T) (400 × 400 matrix, voxel size = .6 mm × 2.93 mm × .6 mm, gap = 1 mm, number of slices = 16, TE = 59 ms, TR = 9534 ms) in a single 42 year old Caucasian male participant using gradient spin echo magnetic resonance imaging (GRASE) and a sequence specifically designed to optimally resolve the BNST in contrast to nearby structures by creating clear contrast between gray matter, white matter, and cerebrospinal fluid (CSF) (Fig. 1). The partial-brain GRASE image was resampled (.6 mm isotropic), coregistered to the participant's T1-weighted (T1W) whole-brain image using SPM8, normalized to standard MNI space by applying normalization parameters created during T1-to-MNI normalization in SPM8, and carefully visually inspected to ensure accurate normalization (Supplementary Fig. 1). To standardize the analysis across scans, we created a single BNST template mask from the normalized high-resolution GRASE image. The BNST was manually traced using 3DSlicer (version 3.4; www.slicer.org) (Fedorov et al., 2012), a software package that provides simultaneous visualization in all orientations. Tracing was performed by JUB and confirmed by SNA and JAC. The anatomical location of the BNST was identified based on a standard brain atlas (Mai et al., 2008). The BNST was initially traced in the coronal view, with the axial and the sagittal views used for confirmation. The GRASE sequence used for the 7 T scan, combined with the high resolution, provided excellent gray/white/CSF separation that was essential for identifying the boundaries of the BNST. The anterior boundary of the BNST was defined as 3 slices (1.8 mm) anterior to the slice containing the anterior commissure. The posterior boundary was defined by the most anterior portion of the internal segment of the globus pallidus. The medial border was defined by the fornix and the lateral border was defined by the internal capsule. The superior border was defined by the lateral ventricle. The inferior border was defined anteriorly by the anterior commissure and posteriorly by the hypothalamus. Although it was not possible to exactly identify each participant's BNST from the T1W images, we visually inspected the placement of the BNST mask on each individual's structural T1W image in 3-D slicer. To assess placement, we checked the BNST mask against three anatomical boundaries that are visible on the T1W images: the anterior commissure, the internal capsule, and the fornix. If the normalization of the BNST mask is accurate, we would expect the BNST mask to sit within those boundaries on each participant's image. The anterior commissure should provide the ventral border for the anterior BNST, the internal capsule should provide the lateral border for the middle portion of the BNST, and the fornix should provide the medial boundary for the lower portion of the BNST. Although the lateral ventricle is also visible, the gray matter/CSF contrast was insufficient to clearly assess the boundary. Based on the visual inspection of the BNST mask according
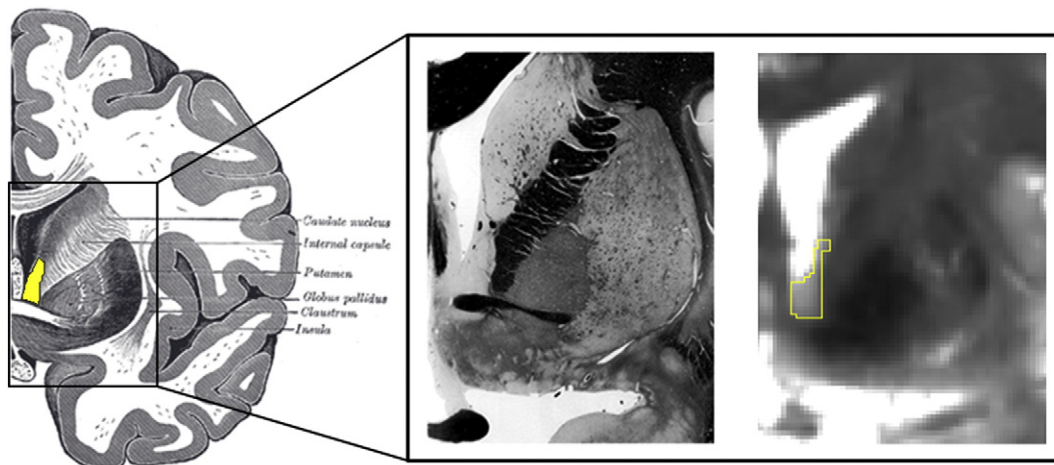
Fig. 1. The human bed nucleus of the stria terminalis (BNST). The human brain is shown as an illustration (Gray, 1918) with the BNST highlighted in yellow. For reference, a similar slice is shown for fixed tissue (Mai et al., 2008). The traced BNST mask used for this study is outlined in yellow (right) on a 7 T gradient spin echo (GRASE) magnetic resonance image.
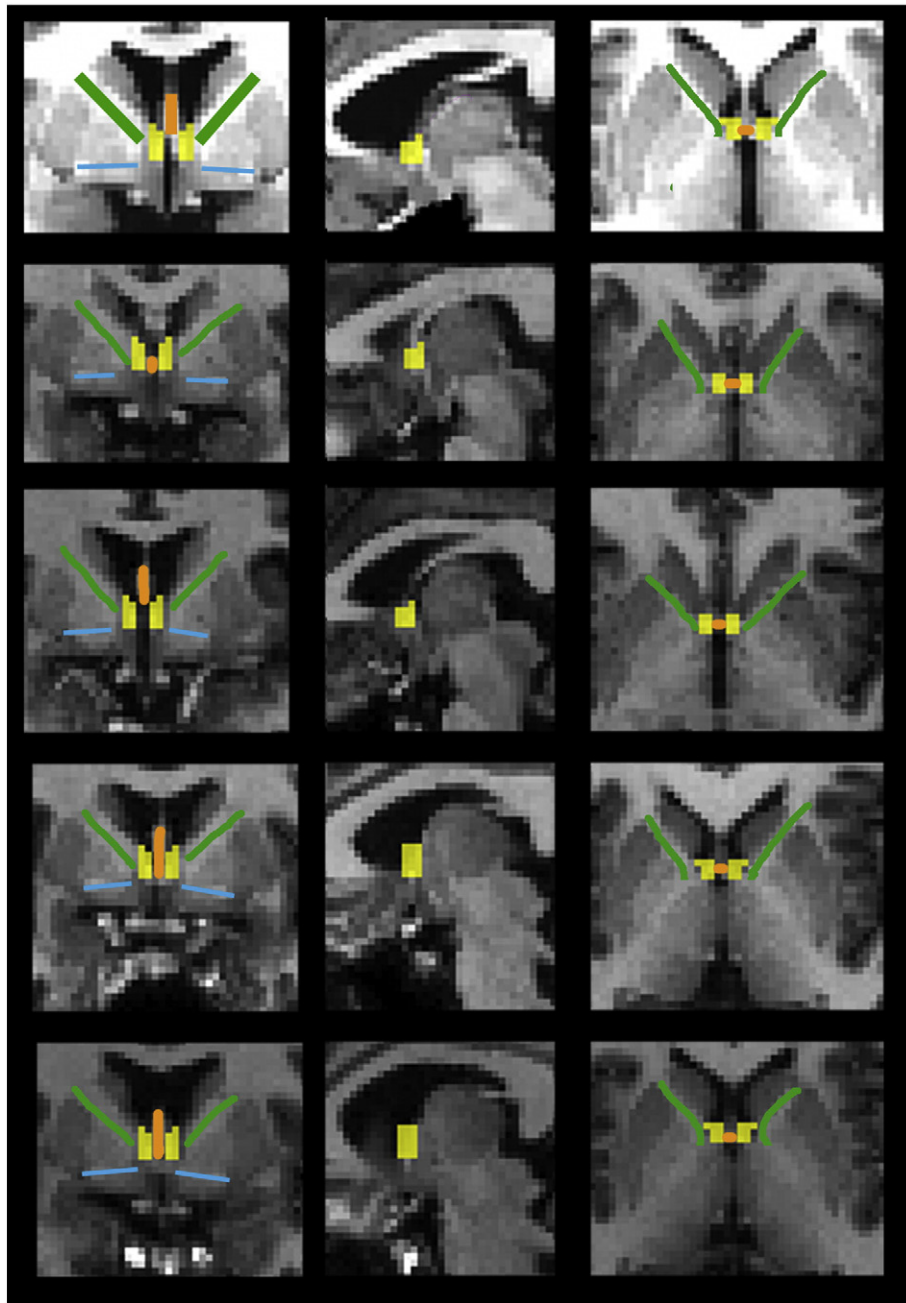
Fig. 2. The traced BNST mask is shown in yellow on a template brain (top row) and on four individual participant brains (rows 2 through 5). The anatomical landmarks used to confirm correct placement within known boundaries are shown in green (internal capsule), orange (fornix), and blue (anterior commissure).

to the visible boundaries, the BNST mask appeared to be appropriately sized and within the boundaries of the BNST for all participants (see Fig. 2 for examples).

Structural connectivity data—image acquisition

Diffusion MRI data were acquired on two identical 3 T Philips Achieva MRI scanners (Philips Healthcare, Inc.). Whole-brain diffusion weighted images were acquired using a pulsed-gradient spin echo, echo-planar imaging (single-shot EPI) pulse sequence and the following parameters: 96 × 96 matrix; voxel size = 2.5 mm isotropic; number of slices = 50; TE = 65 ms; TR = 8.5 s; SENSE acceleration factor = 2. We acquired 92 diffusion directions with a *b* value of 1600 s/mm^2 and one T2-weighted volume with a *b* value of 0 s/mm^2. High-resolution T1W anatomical images were collected with the following parameters:

FOV = 256 mm; number of slices = 170; voxel size = 1 mm isotropic; gap = 0 mm.

Structural connectivity data—image preprocessing

Diffusion weighted data were preprocessed and analyzed using the FMRIB Software Library (FSL, version 4.1.4; Oxford Centre for Functional MRI of the Brain (FMRIB), UK; http://www.fmrib.ox.ac.uk/fsl/) and Matlab (Version R2010, The MathWorks, Inc., Natick, MA). Diffusion data were corrected for eddy current distortions and motion using the Eddy Current Correction tool within the FMRIB FDT toolbox (version 2.0), skull stripped using the FMRIB Brain Extraction tool (BET) (Smith, 2002), and visually inspected for processing artifacts (e.g., skull stripping failure). Diffusion tensors were fitted at each voxel using the FMRIB FDT toolbox. Diffusion data were selected from an original

sample of 135 participants. Scans were first carefully visually inspected for acquisition artifacts (i.e., ghosting, water-fat shift artifacts), and 45 diffusion scans were excluded as a result of artifact detection. Next, 8 participants were excluded for excessive motion, which was defined as greater than 5 mm or 3° of motion in any direction across the 14 min, 36 s diffusion series. Finally, preprocessed scans were visually inspected for processing failures (e.g., skull stripping failure), and all failures at this stage were corrected. This resulted in a final sample of 82 high quality DTI scans in the final analysis.

Structural connectivity data—probabilistic tractography

Because we were interested in describing connectivity across the entire human brain, we used an agnostic exploratory approach with respect to potential BNST connectivity, selecting 54 bilateral target regions (108 total) from the Harvard-Oxford Cortical (n = 47 targets) and Subcortical (n = 7 targets) Probabilistic Atlases (Desikan et al., 2006) representing the entire brain. Probabilistic tractography was used to determine the likelihood of structural connections between the BNST and each target region. Because anatomical tracer studies have shown predominantly ipsilateral connections between the BNST and other gray matter regions (Coolen and Wood, 1998; Sun et al., 1991; Wood and Swann, 2005), separate tractography analyses were conducted for the left and right hemispheres. The few studies which have examined contralateral projections identified only small, midline structures not available in the Harvard-Oxford atlases, such as the mid-brain and brainstem nuclei, and hypothalamus (Dong and Swanson, 2006c; Dong et al., 2000). For each hemisphere, the BNST was seeded for probabilistic tractography to the 54 cortical and subcortical target regions using the following parameters: 5000 streamline samples per voxel, 0.5 mm step lengths, and curvature threshold = 0.2. Standard FSL procedures effectively constrain tractography results by excluding streamlines that enter areas of high uncertainty (i.e., low fractional anisotropy) or are forced to make anatomically improbable decisions (e.g., making a sharp turn or looping back); therefore, additional thresholding of fractional anisotropy values was not performed. The number of tractography streamlines passing from each BNST seed voxel into each target region was recorded. To eliminate spatial overlap between targets, target regions were thresholded at 50% probability and warped to each participant's native diffusion space for probabilistic tractography analysis. The template BNST mask was also warped to each participant's native diffusion space. Because DTI-based tractography methods tend to lose fibers along the track pathways and underestimate connectivity for longer tracts, we applied a distance correction. The distance correction accounts for increased difficulty in hitting targets based on distance from the seed by multiplying the number of target hits by the average distance of the tract. To account for the effect of both seed and target size on accuracy, seed-to-target

probability maps were corrected for size of each target region and individual differences in BNST size. Finally, to minimize the effect of outliers, the seed-to-target probability maps were thresholded at the 5th and 95th percentiles of the mean (i.e., trimmed mean).

Structural connectivity data—validation analyses

We performed two validation analyses: 1) we tested for probabilistic tractography streamlines within the stria terminalis, and 2) we tested connectivity in *a priori* positive and negative control regions selected from the Harvard-Oxford Probabilistic Atlas target masks.

The stria terminalis is a distinct white matter pathway that provides the major connection between the amygdala and the BNST (Fig. 3). Because we would expect to observe tractography streamlines coursing from the BNST through the stria terminalis, we conducted a region of interest analysis within the stria terminalis. The stria terminalis was traced in 3D Slicer (http://www.slicer.org) (Fedorov et al., 2012) with respect to its known anatomical boundaries (Mai et al., 2008). Tracing was performed by JUB and confirmed by SNA and JAC. The stria terminalis was initially traced in the coronal view and confirmed in the sagittal view. The stria terminalis was identified as beginning at the BNST and tracing of the full white matter pathway was performed by following the movement of the white matter tract from slice to slice, ensuring separation from the fornix. The amygdala marked the end of the stria terminalis tracing. The contiguous connection of the pathway was confirmed in sagittal slices. While significant measures were taken to accurately identify the stria terminalis, we acknowledge that manual tracing of this small white matter path may be prone to error.

Each participant's probabilistic tractography pathway map, created as a result of the BNST-to-targets analysis, was thresholded for error (≤1%), warped to MNI space and averaged into a group map. The probabilistic tractography group mask was thresholded at >50% group overlap and masked with the traced stria terminalis mask (Fig. 3). There was a 100% overlap between the group streamline map and our traced stria terminalis mask, indicating that every stria terminalis voxel had probabilistic tractography streamlines running through it and confirming that, on the whole, tractography streamlines were following appropriate anatomical pathways. In order to examine consistency across participants, each individual's probabilistic tractography pathway map was masked with the traced stria terminalis mask, using a stringent individual level thresholding (<1% of total tractography streamlines sent). Almost all (94%) of individuals showed tractography streamlines running through the stria terminalis, again confirming that on the whole tractography streamlines followed appropriate anatomical pathways.

Next, we performed a control region analysis. We chose the amygdala as the positive control region because anatomical studies in rodents and non-human primates have described extensive
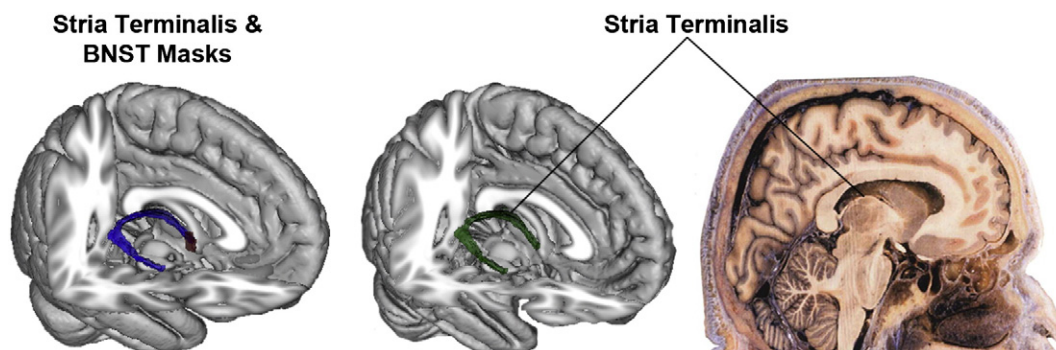
Fig. 3. The stria terminalis mask (blue) and BNST mask (red) are shown on a 3-dimensional template brain (left). The group DTI streamlines map, masked by the stria terminalis mask, is shown in green on a 3-dimensional template brain (middle). Each voxel of the stria terminalis mask overlapped with the group streamlines map, demonstrating that tractography streamlines were coursing through the entire stria terminalis. For reference, a histological section of the stria terminalis is shown (right).

connections between the BNST and amygdala (Coolen and Wood, 1998; Price and Amaral, 1981). Because there are so few primate tracer studies, we selected the negative control region based on known structural brain connections with the amygdala, a region with similar connections as the BNST. The middle frontal gyrus served as the negative control region because it has only sparse connections with the amygdala (Ghashghaei et al., 2007). The amygdala (positive control) was significantly connected with the BNST, while the middle frontal gyrus (negative control) was not significantly connected, demonstrating that probabilistic tractography can accurately discriminate between highly likely and highly unlikely structural connections.

Functional connectivity data—image acquisition

Seven minutes of rs-fMRI data was obtained approximately 20 min after entering the 3 T scanner, following T1W structural image collection, but before DTI data collection (see Structural connectivity data—image acquisition). Participants were instructed to relax and close their eyes, but not fall asleep. Functional images were acquired using an echo-planar imaging sequence with the following parameters: volumes = 203; TR = 2 s; TE = 34 ms; SENSE = 1.8; FOV = 240 mm; and matrix = 80×80. Each volume contained 28 4 mm slices (acquisition voxels = 3 mm × 3 mm × 4 mm) and provided whole-brain coverage. No tasks were performed prior to the collection of the rs-fMRI data.

Functional connectivity data—image preprocessing

Data were preprocessed in SPM8 (http://www.fil.ion.ucl.ac.uk/spm/software/spm8/). Each participant's T1W structural image was segmented into gray matter, white matter, and cerebrospinal fluid using the Voxel-Based Morphometry, 8.0, toolbox (http://dbm.neuro.uni-jena.de/vbm) and gray matter images were normalized to the Montreal Neurological Institute (MNI) gray matter template. Functional data were slice time corrected, motion corrected, coregistered to the segmented gray matter image, and normalized using parameters derived from normalization of the gray matter image. Images were then resampled to 3 mm × 3 mm × 3 mm. Given the small size of the BNST and need for precision in the connectivity analyses, only minimal spatial smoothing was applied (3-mm FWHM). Resting state data were selected from an original sample of 135 participants (same initial sample as diffusion data), using a five-step process to check for image quality. The resting state data were not available at the time of analysis for seven participants. FMRI data were initially selected based on ratings from an in-house quality assurance toolbox used in a previous study (Woodward et al., 2012). The threshold values for poor quality were based on subjective rater agreement of poor quality images on a training dataset of 84 participants, classification based on a fuzzy clustering algorithm and validation on an independent dataset. The thresholds for poor quality are: signal-to-noise ratio (<29), percent standard deviation (>5), percent standard deviation histogram (>.78), percent drift (>1.18), percent fluctuation (>.51), and spatial correlation variance ratio (>.19). Four participants (3%) were removed based on poor quality data. Next, scans were manually inspected and excluded for visual artifacts; 16 participants were excluded due to artifacts. Next, motion was assessed, and any participants with motion greater than 2 mm or 2° in any direction were excluded; eight participants were excluded due to motion. Finally, normalization of the structural and functional data was inspected; one participant was excluded due to poor quality normalization. These exclusions resulted in a final sample of 99 participants with high quality rs-fMRI data.

Functional connectivity data—connectivity analyses

The CONN toolbox (Whitfield-Gabrieli and Nieto-Castanon, 2012), implemented in Matlab, was used to estimate functional connectivity

for each participant. The right and left BNST masks were entered as seed regions. For each participant, the blood-oxygenation-level-dependent (BOLD) time series was estimated as the average time series for all voxels in the left and right BNST seed masks separately. Time series at each voxel had white matter, cerebrospinal fluid, and motion-related signals removed via regression (Behzadi et al., 2007; Chai et al., 2012) and were filtered to 0.1–1.0 Hz to retain the frequencies relevant for connectivity estimation. Global signal was not removed given concerns about the impact of removing global signal on resting state correlations (Murphy et al., 2009; Saad et al., 2012). Temporal correlations were estimated between the average time course from each seed region and all voxels in the brain, producing beta images for each seed region for each participant. The resulting beta images were used for all subsequent analyses.

For consistency with the structural connectivity analyses, average positive connectivity for each of the 54 target regions from the Harvard-Oxford Cortical and Subcortical Probabilistic Atlases (Desikan et al., 2006) (Table 1) was estimated. Target regions were thresholded at 50% probability to remove overlap between regions. Positive connectivity maps were created for each participant. Average connectivity between the BNST and each target region was extracted using SPM8.

To explore the spatial pattern across each voxel in the brain, we also conducted a voxel-wise functional connectivity analysis. The left and right BNST were the seed regions for the left and right hemispheres, respectively.

Statistical analysis of connectivity

Structural and functional connectivity values are inherently descriptive, preventing any determination of whether a specific region is definitively connected to the BNST. For this initial characterization of BNST connectivity, we took a conservative approach with the goal of determining the target regions with the highest likelihood of structural or functional connectivity. We performed a bootstrap analyses (10,000 permutations) to identify the 95% confidence interval around the mean and defined a significant likelihood of a connection as a connectivity value greater than the upper limit of the 95% confidence interval (structural connectivity = .077; functional connectivity = .117). Furthermore, to ensure that significant values for target regions were not driven by a small percentage of participants, only significant regions where more than 50% of participants were above the threshold value are reported. For the whole-brain functional connectivity analysis, we used a conservative t-value of >8.0 and a cluster threshold of 20 voxels (540 mL) to identify significant clusters.

Spatial pattern of connectivity

To explore the spatial pattern of BNST structural connectivity within each significant target, we conducted post-hoc probabilistic tractography analyses. Each target identified as having a significant likelihood of connection with the BNST was seeded for probabilistic tractography to the BNST (5000 streamline samples per voxel, 0.5 mm step lengths, curvature threshold = 0.2, with correction for distance), and the number of tractography streamlines passing from each target seed voxel into the BNST was recorded. Each participant's target-to-BNST probability maps were thresholded at the 5th and 95th percentiles of the mean to exclude outlier values, warped to MNI space, and averaged across participants in order to observe the average spatial pattern of BNST structural connectivity across the group.

To explore the spatial pattern of BNST functional connectivity, we conducted a functional connectivity analysis within each significant target region. BNST functional connectivity was conducted for each participant. Individual participant BNST maps were entered into a one-sample t-test and masked by the significant target regions in order to illustrate the average spatial pattern of BNST functional connectivity.

Table 1
Mean connectivity values and % connectivity by target region.

Harvard-Oxford cortical and subcortical target masks	DTI connectivity value	% Subjects with DTI connectivity	RS-fMRI connectivity value	% Subjects with RS connectivity
Left accumbens	**0.4232**	**99%**	**0.2507**	**71%**
Right accumbens	**0.3429**	**95%**	**0.2397**	**67%**
Left amygdala	**0.3858**	**100%**	**0.1333**	44%
Right amygdala	**0.2712**	**94%**	**0.1256**	44%
Left angular gyrus	0.0140	2%	0.1020	35%
Right angular gyrus	0.0073	0%	0.1019	34%
Left caudate	**0.2034**	**100%**	**0.2613**	**91%**
Right caudate	**0.1108**	**87%**	**0.2646**	**88%**
Left central operculum cortex	0.0072	1%	0.1065	38%
Right central operculum cortex	0.0045	0%	0.0885	28%
Left cingulate gyrus, anterior	0.0243	5%	**0.1212**	44%
Right cingulate gyrus, anterior	0.0126	2%	0.1114	39%
Left cingulate gyrus, posterior	0.0296	6%	0.1125	42%
Right cingulate gyrus, posterior	0.0270	4%	0.0972	28%
Left cuneal cortex	0.0409	11%	0.0784	24%
Right cuneal cortex	0.0256	6%	0.0707	22%
Left frontal medial cortex	0.0460	20%	**0.1385**	49%
Right frontal medial cortex	0.0325	11%	0.1107	33%
Left frontal operculum cortex	0.0466	13%	0.1149	38%
Right frontal operculum cortex	0.0215	5%	0.0969	29%
Left frontal orbital cortex	0.0428	12%	0.1142	40%
Right frontal orbital cortex	0.0341	10%	0.1096	43%
Left frontal pole	0.0623	24%	0.1135	36%
Right frontal pole	0.0382	1%	0.1039	37%
Left Heschl's gyrus	0.0134	4%	**0.1306**	40%
Right Heschl's gyrus	0.0171	4%	0.1086	35%
Left hippocampus	**0.2472**	**77%**	**0.1319**	**56%**
Right hippocampus	**0.2527**	**84%**	**0.1224**	44%
Left inferior frontal gyrus, pars opercularis	0.0256	5%	**0.1219**	42%
Right inferior frontal gyrus, pars opercularis	0.0171	4%	0.1113	36%
Left inferior frontal gyrus, pars triangularis	**0.1274**	32%	**0.1294**	43%
Right inferior frontal gyrus, pars triangularis	0.0537	7%	0.1098	39%
Left inferior temporal gyrus, anterior	0.0626	23%	0.0996	30%
Right inferior temporal gyrus, anterior	0.0312	10%	0.0892	26%
Left Inferior temporal gyrus, posterior	0.0353	12%	0.0981	28%
Right inferior temporal gyrus, posterior	0.0270	10%	0.1040	35%
Left inferior temporal gyrus, temporooccipital	0.0385	13%	0.1035	27%
Right inferior temporal gyrus, temporooccipital	0.0260	5%	0.0894	33%
Left insular cortex	0.0221	2%	0.1142	37%
Right insular cortex	0.0258	7%	0.1006	31%
Left intracalcarine cortex	0.0454	16%	0.1030	33%
Right intracalcarine cortex	0.0153	2%	0.1009	30%
Left lateral occipital cortex, inferior	0.0174	1%	0.0944	27%
Right lateral occipital cortex, inferior	0.0224	9%	0.0906	32%
Left lateral occipital cortex, superior	0.0204	4%	0.1060	41%
Right lateral occipital cortex, superior	0.0193	1%	0.0981	31%
Left lingual gyrus	0.0369	9%	0.0980	35%
Right lingual gyrus	0.0264	7%	0.0893	31%
Left middle frontal gyrus	0.0197	9%	**0.1202**	41%
Right middle frontal gyrus	0.0076	0%	**0.1206**	46%
Left middle temporal gyrus, anterior	0.0658	20%	0.1135	41%
Right middle temporal gyrus, anterior	0.0385	15%	0.1027	38%
Left middle temporal gyrus, posterior	0.0125	5%	0.1050	32%
Right middle temporal gyrus, posterior	0.0197	2%	0.1013	30%
Left middle temporal gyrus, temporooccipital	0.0173	4%	0.1102	36%
Right middle temporal gyrus, temporooccipital	0.0133	0%	0.0951	28%
Left occipital fusiform gyrus	0.0483	15%	0.0866	26%
Right occipital fusiform gyrus	0.0408	11%	0.0888	28%
Left occipital pole	0.0242	6%	0.0978	28%
Right occipital pole	0.0184	2%	0.0943	31%
Left pallidum	**0.2134**	**100%**	0.1123	41%
Right pallidum	**0.1719**	**90%**	**0.1208**	**51%**
Left paracingulate gyrus	0.0208	2%	**0.1382**	**51%**
Right paracingulate gyrus	0.0109	0%	**0.1210**	40%
Left parahippocampal gyrus, anterior	0.0667	21%	0.1020	29%
Right parahippocampal gyrus, anterior	0.0633	24%	0.1067	39%
Left parahippocampal gyrus, posterior	0.0598	23%	0.1089	39%
Right parahippocampal gyrus, posterior	**0.0828**	28%	0.0998	30%
Left parietal operculum cortex	0.0181	5%	0.0915	29%
Right parietal operculum cortex	0.0108	0%	0.0944	31%
Left planum polare	0.0895	37%	0.1002	35%
Right planum polare	0.0598	24%	0.0996	36%
Left planum temporale	0.0233	9%	0.1164	40%
Right planum temporale	0.0307	10%	0.0963	30%
Left postcentral gyrus	0.0164	0%	0.1037	36%

Table 1 (*continued*)

Harvard-Oxford cortical and subcortical target masks	DTI connectivity value	% Subjects with DTI connectivity	RS-fMRI connectivity value	% Subjects with RS connectivity
Right postcentral gyrus	0.0187	2%	0.0881	29%
Left precentral gyrus	0.0180	6%	0.1103	33%
Right precentral gyrus	0.0224	9%	0.0980	30%
Left precuneous cortex	0.0196	2%	0.0935	32%
Right precuneous cortex	0.0187	2%	0.0854	28%
Left putamen	**0.1663**	**93**%	**0.1387**	**60**%
Right putamen	**0.1437**	**84**%	**0.1453**	**55**%
Left subcallosal cortex	0.0971	**52**%	**0.1249**	44%
Right subcallosal cortex	**0.1239**	**56**%	0.1092	38%
Left sup frontal gyrus	0.0457	13%	**0.1203**	39%
Right sup frontal gyrus	0.0257	5%	0.1059	37%
Left superior temporal gyrus, anterior	0.0482	12%	0.0982	28%
Right superior temporal gyrus, anterior	0.0480	9%	0.0898	31%
Left superior parietal lobule	0.0441	16%	0.0787	25%
Right superior parietal lobule	0.0262	5%	0.0797	25%
Left supplementary motor cortex	0.0136	0%	0.0924	33%
Right supplementary motor cortex	0.0120	2%	0.0905	27%
Left supracalcarine cortex	0.0415	11%	0.0793	25%
Right supracalcarine cortex	0.0400	12%	0.0797	25%
Left supramarginal gyrus, anterior	0.0104	0%	0.1032	33%
Right supramarginal gyrus, anterior	0.0143	2%	0.0911	29%
Left supramarginal gyrus, posterior	0.0179	4%	0.1042	33%
Right supramarginal gyrus, posterior	0.0164	2%	0.1066	37%
Left temporal fusiform cortex, anterior	0.0904	22%	0.0826	27%
Right temporal fusiform cortex, anterior	**0.1630**	29%	0.0958	27%
Left temporal fusiform cortex, posterior	0.0603	13%	0.0930	28%
Right temporal fusiform cortex, posterior	0.0584	22%	0.0950	29%
Left temporal occipital fusiform gyrus	0.0360	12%	0.0888	28%
Right temporal occipital fusiform gyrus	0.0338	11%	0.0834	26%
Left temporal pole	**0.1191**	**60**%	0.0995	33%
Right temporal pole	0.0934	40%	0.0952	27%
Left thalamus	**0.1233**	**83**%	**0.1458**	**57**%
Right thalamus	**0.0895**	**59**%	**0.1446**	**63**%

The bold values reach the significance criterion (95th percentile) or the % subjects criterion (> 50%).

Amygdala subnuclei connectivity

The amygdala is composed of multiple distinct subnuclei, and human imaging studies have confirmed differential patterns of structural and functional connectivity across amygdala subnuclei (Bach et al., 2011; Etkin et al., 2009; Mishra et al., 2013; Roy et al., 2009). Anatomical tracer studies in both rodents and non-human primates have demonstrated that the BNST has different patterns of connectivity with amygdala subnuclei (Coolen and Wood, 1998; Dong et al., 2001a; Price and Amaral, 1981). For example, the BNST has strong, dense connections with the centromedial subnucleus of the amygdala (Price and Amaral, 1981), but weaker, more diffuse connections with other amygdala subnuclei (Dong et al., 2001a). To determine whether the same pattern exists in humans we performed two analyses. Amygdala subnuclei were identified using a probabilistic atlas (Amunts et al., 2005), thresholded at 50% with each voxel assigned to the subnuclei with the greatest probability of membership. Structural and functional connectivity between the left and right BNST and the ipsilateral amygdala subnuclei were calculated. First, we tested whether each subnucleus had a significant likelihood of connectivity using the critical values from the previous bootstrap analyses. Second, we directly tested for differences in the strength of connectivity between the three subnuclei by comparing pairs of subnuclei using permutation *t*-tests (10,000 permutations, α = .05). Tests were performed using an in-house script written in R (R Core Development Team, 2008) according to standard methods (Good, 2000).

Sex differences

The BNST is sexually dimorphic in rodents (Hines et al., 1985, 1992) and may also be dimorphic in humans (Allen and Gorski, 1990; Chung et al., 2002); however, very little research has investigated whether dimorphic differences translate to altered BNST connectivity. Sex differences in structural and functional connectivity were tested using permutation *t*-tests (10,000 permutations, α = .05). To minimize the potential for type I error due to multiple testing, analyses were restricted to the regions that were identified as having as significant probability of being connected with the BNST in the previous structural and functional analyses.
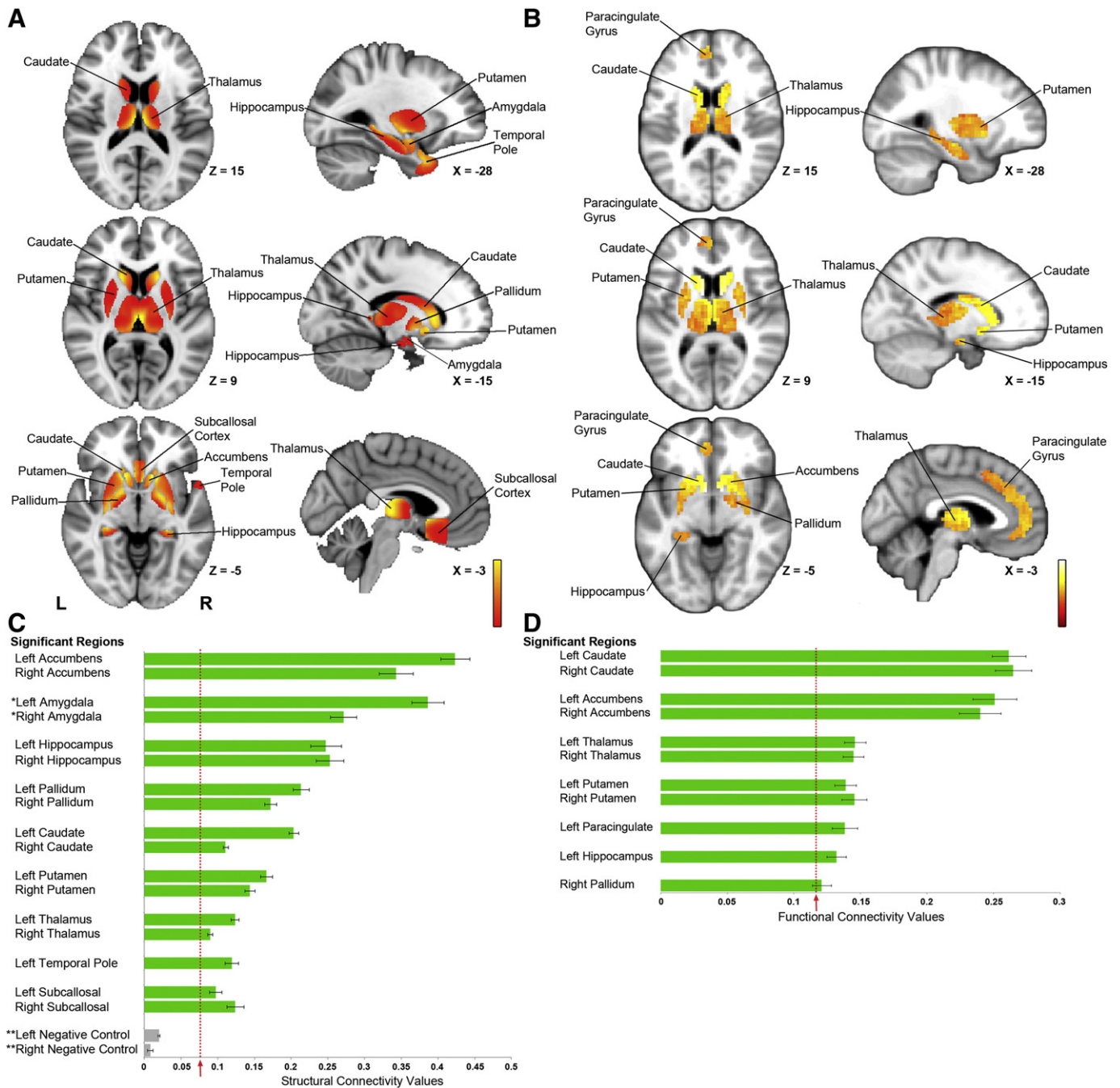
Results

Structural and functional connectivity of the BNST

Of the 108 target regions tested using structural connectivity, 17 regions showed significant likelihood of structural connectivity with the BNST (Figs. 4A, C). As expected, these included several regions of the basal ganglia (accumbens, caudate, putamen, and pallidum), limbic system (amygdala, subcallosal cortex, and hippocampus), and thalamus, indicating evolutionarily-conserved connections across species. We also identified a connection with the temporal pole which has not been previously described in rodents.

Of the 108 target regions tested using functional connectivity, 11 regions showed significant likelihood of functional connectivity with the BNST (Figs. 4B, D). These included several regions of the basal ganglia (accumbens, caudate, putamen, and pallidum), limbic system (hippocampus), and thalamus, replicating findings using anatomic tracer studies in rodents as well as our DTI findings. Functional connectivity identified one novel target region of the BNST, the paracingulate gyrus.

In order to further explore functional connectivity patterns across the entire brain, we conducted a post-hoc voxel-wise functional connectivity analysis. The findings from the whole-brain functional connectivity analysis were consistent with the results from the target region analysis. Significant BNST connectivity was observed with the basal ganglia, hippocampus, thalamus, and paracingulate gyrus. The whole-brain approach also identified some additional regions not shown in the target region approach, including other limbic regions (amygdala,

Fig. 4. Structural and functional connectivity of the bed nucleus of the stria terminalis (BNST) in the human brain. Voxel-wise connectivity maps shown on a template brain illustrate spatial patterns of structural (A) and functional connectivity (B) within regions identified as having significant likelihood of connectivity with the BNST. Color bars indicate strength of connectivity with lighter colors representing stronger connectivity. Using DTI (n = 82) and rs-fMRI (n = 99) to assess structural and functional BNST connectivity, respectively, a varied pattern of BNST spatial connectivity is demonstrated within each larger target region. Bar graphs show mean connectivity values by region for structural (C) and functional (D) analyses, with error bars representing the standard error of the mean. The vertical dotted line indicates the threshold of significant likelihood of connectivity as determined using bootstrap methods (10,000 permutations, >95% confidence interval of the mean). Target regions were determined to have a significant likelihood of connectivity with the BNST if 1) the mean connectivity value passed the threshold for significance (structural connectivity >.077, functional connectivity >.117), and 2) at least 50% of individual connectivity values passed the threshold for significance (DTI, n > 40; rs-fMRI, n > 49). Out of 108 regions tested, 17 regions passed both threshold criteria for significant structural connectivity (C) and 11 regions passed both threshold criteria for significant functional connectivity (D). Note: *Amygdala = positive control region in the structural connectivity analysis; ** Middle frontal gyrus = negative control region in the structural connectivity analysis.

subcallosal cortex, parahippocampal gyrus, and anterior insula), prefrontal cortex regions (anterior cingulate cortex, medial frontal gyrus, superior frontal gyrus, inferior frontal gyrus, and middle frontal gyrus), posterior cingulate cortex, calcarine fissure, precuneus, and precentral gyrus (Fig. 5).

Spatial pattern of connectivity

Next, because target regions were relatively large and distinct patterns of connectivity may exist within each region, we explored the spatial pattern of BNST connectivity by performing post-hoc
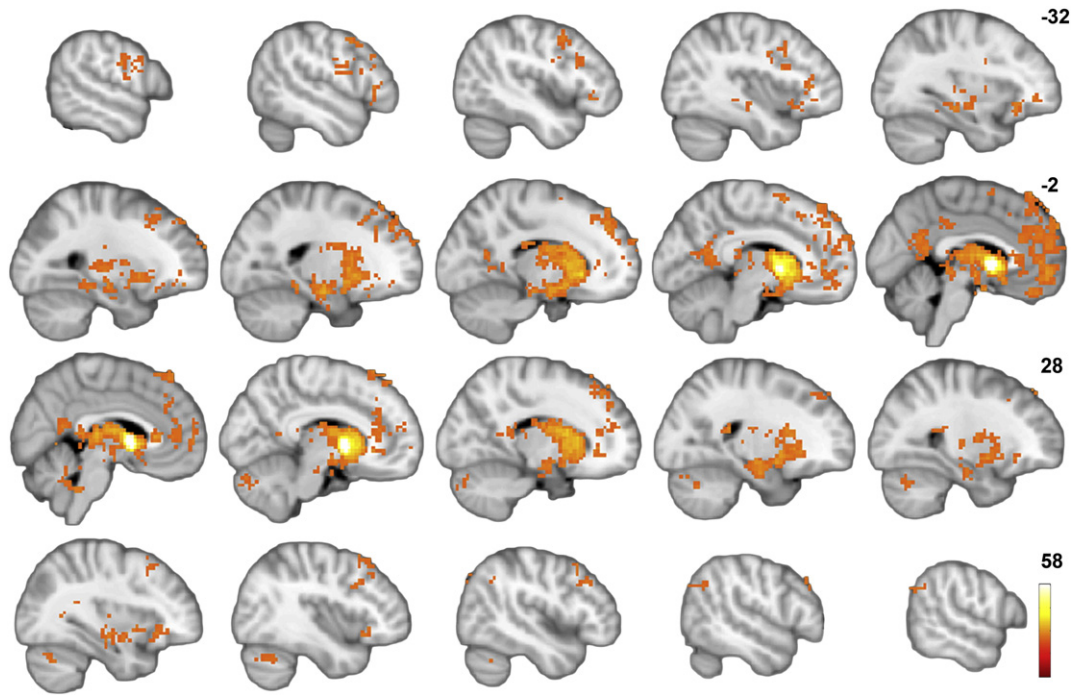
Fig. 5. Exploratory voxel-wise functional connectivity findings. The results of this voxel-wise analysis were consistent with the results from the target region analysis, identifying large clusters within each of the significant target regions. The voxel-wise analysis also revealed significant functional connectivity within regions which were not identified using the target region approach, including limbic regions (amygdala, subcallosal cortex, parahippocampal gyrus, and anterior insula), prefrontal cortex regions (anterior cingulate cortex, medial frontal gyrus, superior frontal gyrus, inferior frontal gyrus, and middle frontal gyrus), posterior cingulate cortex, calcarine fissure, precuneus, and precentral gyrus.

analyses within each of the significant target regions. Each target region showed a distinct spatial pattern of structural connectivity with the BNST, ranging from low to high connectivity (Fig. 4A). Functional connectivity also showed a distinct spatial pattern of connectivity within each target region (Fig. 4B). Several regions showed a similar spatial pattern of connectivity across both structural and functional analyses; for example, the head of the caudate and the medial thalamus showed

stronger structural and functional connectivity than the tail of the caudate and the lateral thalamus, respectively.

Amygdala subnuclei–structural and functional connectivity

In rodents, the BNST is differentially connected with the subnuclei of the amygdala (Coolen and Wood, 1998; Dong et al., 2001a; Price and
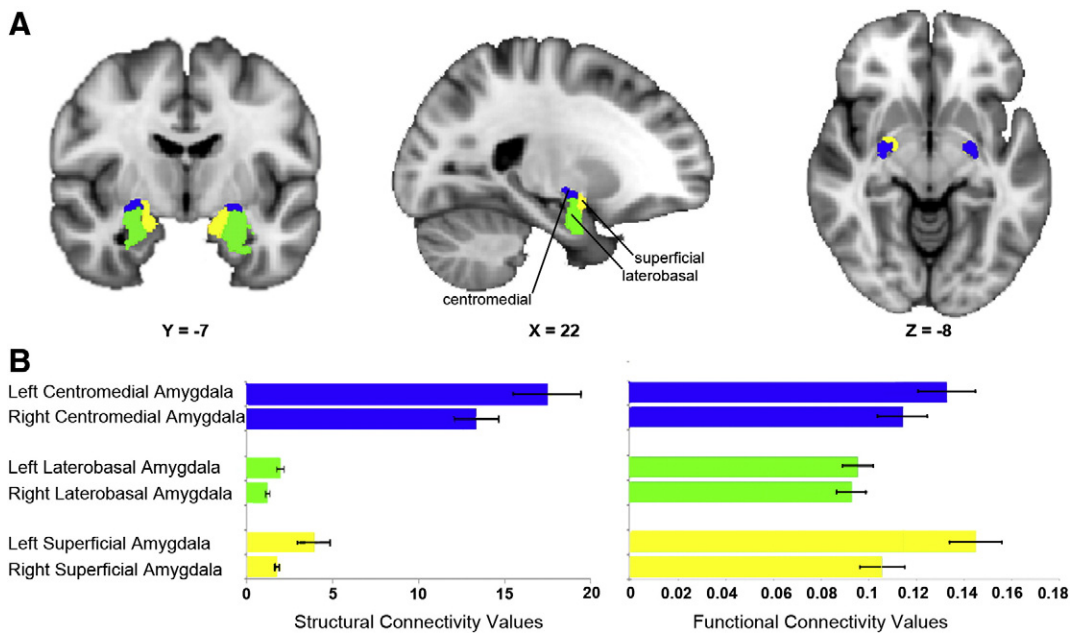
Fig. 6. Differential structural and functional connectivity of amygdala subnuclei. An illustration of the three amygdala subnuclei is shown on a template brain in coronal, sagittal, and axial slices (A). Bar graphs show strength of structural (B, left) and functional (B, right) bed nucleus of the stria terminalis (BNST) connectivity by amygdala subnuclei, with error bars representing the standard error of the mean. The centromedial amygdala had greater structural connectivity with the BNST compared to both the laterobasal and superficial subnuclei (p's < .001) (B, left). BNST functional connectivity was greater for the left and right superficial subnuclei, compared with the left and right laterobasal subnuclei (left: p < .001, right: p = .002) and the left centromedial subnucleus (p = .026) (B, right).

Amaral, 1981); therefore we identified which subnuclei showed evidence for connectivity and directly tested for differences in connectivity across the three subnuclei (centromedial, superficial, and laterobasal). All three subnuclei had a significant likelihood of structural connectivity and the centromedial and superficial subnuclei also had a significant likelihood of functional connectivity. Directly testing for differences in strength of structural connectivity revealed that BNST structural connectivity was significantly greater for the centromedial amygdala (Fig. 6), compared to both the basolateral and superficial subnuclei, consistent with anatomical tracer studies. BNST functional connectivity was significantly greater for the left and right superficial subnucleus, compared with the left and right laterobasal subnucleus and the left centromedial subnucleus. The centromedial nucleus trended towards significantly greater connectivity than the laterobasal in the right hemisphere.

Sex differences

Across species, the BNST has sexually dimorphic regions which are larger in males than females (Allen and Gorski, 1990; Chung et al., 2002; Hines et al., 1985, 1992). However, the implications of larger volume for connectivity in humans are unknown. We tested for sex differences in structural and functional connectivity in the regions that showed significant connectivity with the BNST. For structural connectivity, 76% of the regions had greater connectivity in females (Table 2). In contrast, for functional connectivity, the left putamen had greater connectivity in males than females, and the right thalamus had significantly greater connectivity in females than males. Because differences in motion could have contributed to the observed sex differences, we compared the two groups on six motion parameters. Males and females had similar motion for both the DTI and rs-fMRI scans (all p > .10).

Table 2
Sex differences in structural and functional connectivity.

	Male mean (SD)	Female mean (SD)	p-value
Structural connectivity target region			
Left accumbens	**.35 (.14)**	**.51 (.18)**	**<.001**
Right accumbens	**.28 (.14)**	**.41 (.25)**	**.005**
Left amygdala	**.34 (.15)**	**.44 (.23)**	**.020**
Right amygdala	**.22 (.10)**	**.34 (.19)**	**.001**
Left hippocampus	**.20 (.15)**	**.30 (.21)**	**.027**
Right hippocampus	**.21 (.16)**	**.30 (.17)**	**.013**
Left pallidum	**.19 (.08)**	**.25 (.25)**	**.004**
Right pallidum	**.15 (.06)**	**.20 (.08)**	**.002**
Left caudate	**.18 (.05)**	**.23 (.06)**	**.001**
Right caudate	**.10 (.03)**	**.12 (.03)**	**.002**
Left putamen	**.14 (.05)**	**.19 (.09)**	**.002**
Right putamen	**.12 (.05)**	**.17 (.07)**	**<.001**
Left thalamus	.12 (.04)	.13 (.05)	.088
Right thalamus	.08 (.02)	.10 (.04)	.062
Left temporal pole	.11 (.09)	.13 (.09)	.283
Left subcallosal cortex	**.08 (.07)**	**.12 (.09)**	**.045**
Right subcallosal cortex	.10 (.09)	.15 (.12)	.065
Functional connectivity target region			
Left accumbens	.26 (.14)	.24 (.18)	.413
Right accumbens	.23 (.16)	.25 (.15)	.715
Left caudate	.25 (.10)	.27 (.15)	.424
Right caudate	.26 (.14)	.25 (.15)	.747
Left hippocampus	.13 (.06)	.13 (.08)	.738
Right pallidum	.13 (.07)	.11 (.08)	.284
Left paracingulate gyrus	.14 (.09)	.14 (.10)	.996
Left putamen	**.16 (.08)**	**.12 (.08)**	**.032**
Right putamen	.13 (.08)	.16 (.10)	.182
Left thalamus	.14 (.07)	.15 (.09)	.509
Right thalamus	**.13 (.06)**	**.16 (.09)**	**.047**

The bold values indicate regions with significant differences.

Discussion

The goal of this study was to describe the structural and functional connectivity of the BNST in humans. Using DTI and rs-fMRI, we provide a preliminary characterization of human BNST neurocircuitry. The BNST was structurally and functionally connected with multiple subcortical regions, including limbic, thalamic, and basal ganglia structures, replicating structural findings in rodents (Dong and Swanson, 2004a, 2006a; Dong et al., 2001b). We also identified two novel connections that have not been previously reported in rodents or non-human primates; the BNST was structurally connected with the temporal pole and was functionally connected with the paracingulate gyrus. The identification of BNST circuitry lays a critical foundation for future studies investigating the neural circuits mediating anxiety and addiction in humans.

Structural and functional findings showed convergence in the accumbens, thalamus, hippocampus, pallidum, caudate, and putamen. This convergence is consistent with previous studies showing that white matter tracts connect commonly identified resting state functional networks (Greicius et al., 2009; Hagmann et al., 2008; van den Heuvel et al., 2009). Given both structural and functional evidence for connectivity, we propose that these regions form the key nodes of a BNST circuit in humans. However, there were also regions that did not show convergence across the connectivity analyses. For example, the amygdala and subcallosal cortex regions showed significant structural, but not functional, connectivity in the primary target region analysis. One possibility for the difference in findings is the conservative statistical approach used to determine connectivity, which required that average connectivity value reach a specific threshold and that at least half of the participants' values also reach that threshold. Both the amygdala and subcallosal cortex met the first criterion, based on average values, but fell just short of the participant-specific criterion (see Table 1); both regions also had clusters with significant connectivity in the exploratory voxel-wise analysis. Another possibility is that functional connections between some regions may be best observed under conditions of stress or anxiety. For example, a recent study in rodents illustrated that the effects of severing structural connections between the BNST and amygdala were only observable following administration of an anxiogenic drug and were not observable at baseline (Cai et al., 2012). Finally, it is possible that some of the observed structural connections may not reflect glutameteric projections but may instead reflect increased GABA projections, which have an unclear effect on fMRI signal (Arthurs and Boniface, 2002).

One of the best-established connections of the BNST is with the central nucleus of the amygdala (CeA). Structural connections have been well-described in both rodents and non-human primates (Coolen and Wood, 1998; Decampo and Fudge, 2013; Dong et al., 2001a; Price and Amaral, 1981). Although a description of structural connections is currently lacking in humans, functional connectivity was recently demonstrated using rs-fMRI (Oler et al., 2012). Here, we confirm those findings and also provide evidence of structural connections between the CeA and BNST in humans. Furthermore, we show that BNST structural connections with the CeA are stronger than connections with the superficial and basolateral nuclei, although we find evidence for structural connectivity across all three subnuclei, similar to non-human primates (Decampo and Fudge, 2013). The lower levels of structural connectivity in the superficial and basolateral subnuclei likely contributed to the amygdala showing the second highest strength of connectivity with the BNST, instead of the first. The distinct pattern of connectivity across amygdala subnuclei has been well-established and may suggest that these subnuclei should be examined separately. We also extended the findings from the previous study by showing functional connectivity between the BNST and the superficial subnucleus of the amygdala. Given that the BOLD signal reflects inputs to a region as well as local processing (Logothetis and Wandell, 2004), the functional connectivity

may reflect connectivity among the amygdala subnuclei in addition to BNST-amygdala connectivity.

While the BNST-amygdala relationship often receives the most attention, the accumbens is also considered to be a part of the 'extended amygdala', a cluster of nuclei that includes the central nucleus of the amygdala, the BNST, and the accumbens (Alheid and Heimer, 1988). In the present study, the BNST-accumbens connection was the strongest structural connection and second strongest functional connection. The structural finding is consistent with anatomical tracer studies in rodents that also show strong structural connectivity (Dong and Swanson, 2004b; Wood and Swann, 2005); however, evidence for the functional role of that connection is lacking. The link between the BNST and accumbens is especially exciting given that both structures have a prominent role in addiction neurocircuitry (Koob and Volkow, 2010).

Of interest, there were two regions that showed BNST connectivity in humans that have not been described in rodents or primates— the temporal pole and the paracingulate gyrus. The temporal pole is a paralimbic region that has bidirectional connections with the basomedial forebrain (Olson et al., 2007). In humans, the medial portion of the temporal pole—the area which showed highest BNST connectivity in our spatial analysis—is akin to the agranular insular cortex in rodents, which has strong connections with the BNST (Reynolds and Zahm, 2005). The paracingulate gyrus showed functional connectivity with the BNST. This finding is intriguing in light of growing evidence that the prefrontal cortex figures prominently in anxiety and addiction disorders (Davidson and Irwin, 1999; Etkin, 2010; Goldstein et al., 2002; Kim et al., 2011; Koob and Volkow, 2010; Shin and Liberzon, 2010). However, the paracingulate gyrus was not structurally connected to the BNST, consistent with previous findings that functional connectivity is not constrained by structural paths (Honey et al., 2009; Koch et al., 2002). Given the lack of direct structural connections, it is likely that the functional connectivity between the BNST and paracingulate gyrus is indirect and transmitted through other brain regions, such as the subcallosal cortex. While these novel connections are intriguing, cautious interpretation is recommended until they are replicated.

Sexually dimorphic brain regions are of special interest given sex differences in the prevalence of anxiety disorders (Lewinsohn et al., 1998; McLean et al., 2011) and addiction (Becker and Hu, 2008). Indeed in rodents, the BNST has been proposed to play an important role in gender-dependent effects of stress on learning (Bangasser, 2013). In the present study we identified several gender differences in BNST structural connectivity, with greater connectivity in females. In contrast, there were few differences in functional connectivity. As described earlier, there are several possible explanations for the differences between the structural and functional findings including the role of context (i.e., resting state vs. anxiety task), and the fact that structural connections may reflect increased GABA projections (Polston et al., 2004), which have an unclear effect on fMRI signal (Arthurs and Boniface, 2002).

This study has several limitations which may be addressed in future research. First, we used a single BNST mask, based on a male participant, for all participants. The use of a single region of interest mask is common in DTI and resting state analyses (Amunts et al., 2005), even for sexually dimorphic brain regions such as the amygdala (Lombardo et al., 2012). This approach allowed us to standardize our analysis across individuals; however, the approach may lack sensitivity to individual differences in anatomy. Although it was not possible to exactly identify the BNST on the T1W structural images, we were able to check the placement of the BNST mask using several anatomical landmarks that are visible on the T1W. One possible implication of using a single mask is that some individuals may have voxels outside of the mask that are truly part of the BNST and other individuals may have voxels inside the mask that are not truly part of the BNST. The implication for either of these cases is decreased power to detect true BNST connections; therefore, the results presented here should be considered preliminary and possibly conservative. Future studies should use the high contrast provided by

the GRASE sequence and the high resolution provided by the 7 T MRI to create a probabilistic atlas of the BNST across a wide range of individuals. Second, we used an MRI atlas (Harvard-Oxford) for our target regions. This atlas does not contain masks for a number of small structures which have been shown to be connected to the BNST in rodents, such as the hypothalamus, substantia nigra, and substantia innominata. Third, DTI studies are susceptible to a proximity bias, whereby there is a greater likelihood to detect connections with more proximal regions. We reduced the likelihood of this bias using a distance correction. Furthermore, although we did observe connectivity with multiple proximal regions, these regions (i.e. accumbens, caudate, putamen, and thalamus) have also been detected in vivo with anatomical tracer studies and in the functional connectivity analysis, which does not suffer from proximity bias. Also, other proximal regions which do not show connectivity with tracer studies also did not show connectivity here (e.g., cingulate gyrus). Fourth, for this initial study of BNST connectivity, we used a relatively conservative statistical approach. The combination of stringent statistical thresholds and the use of target regions may have limited our ability to detect regions with moderate or spatially restricted connectivity with the BNST. Future studies will be needed to confirm and extend these findings.

To our knowledge, this is the first study to characterize BNST structural and functional connectivity in humans. Given the key role that the BNST plays in anxiety and addictive disorders, these results lay the foundation for future studies of psychiatric illness.

Supplementary data to this article can be found online at http://dx.doi.org/10.1016/j.neuroimage.2014.01.017.

Conflict of interest statement

The authors declare no competing financial interests.

References

Alheid, G.F., Heimer, L., 1988. New perspectives in basal forebrain organization of special relevance for neuropsychiatric disorders: the striatopallidal, amygdaloid, and corticopetal components of substantia innominata. Neuroscience 27, 1–39.

Allen, L.S., Gorski, R.A., 1990. Sex difference in the bed nucleus of the stria terminalis of the human brain. J. Comp. Neurol. 302, 697–706.

Alvarez, R.P., Chen, G., Bodurka, J., Kaplan, R., Grillon, C., 2011. Phasic and sustained fear in humans elicits distinct patterns of brain activity. Neuroimage 55, 389–400.

Amunts, K., Kedo, O., Kindler, M., Pieperhoff, P., Mohlberg, H., Shah, N.J., Habel, U., Schneider, F., Zilles, K., 2005. Cytoarchitectonic mapping of the human amygdala, hippocampal region and entorhinal cortex: intersubject variability and probability maps. Anat. Embryol. (Berl) 210, 343–352.

Arthurs, O.J., Boniface, S., 2002. How well do we understand the neural origins of the fMRI BOLD signal? Trends Neurosci. 25, 27–31.

Bach, D.R., Behrens, T.E., Garrido, L., Weiskopf, N., Dolan, R.J., 2011. Deep and superficial amygdala nuclei projections revealed in vivo by probabilistic tractography. J. Neurosci. 31, 618–623.

Bangasser, D.A., 2013. Sex differences in stress-related receptors: "micro" differences with "macro" implications for mood and anxiety disorders. Biol. Sex Differ. 4, 2.

Becker, J.B., Hu, M., 2008. Sex differences in drug abuse. Front. Neuroendocrinol. 29, 36–47.

Behzadi, Y., Restom, K., Liau, J., Liu, T.T., 2007. A component based noise correction method (CompCor) for BOLD and perfusion based fMRI. Neuroimage 37, 90–101.

Cai, L., Bakalli, H., Rinaman, L., 2012. Yohimbine anxiogenesis in the elevated plus maze is disrupted by bilaterally disconnecting the bed nucleus of the stria terminalis from the central nucleus of the amygdala. Neuroscience 223, 200–208.

Chai, X.J., Castañón, A.N., Ongür, D., Whitfield-Gabrieli, S., 2012. Anticorrelations in resting state networks without global signal regression. Neuroimage 59, 1420–1428.

Chung, W.C.J., De Vries, G.J., Swaab, D.F., 2002. Sexual differentiation of the bed nucleus of the stria terminalis in humans may extend into adulthood. J. Neurosci. 22, 1027–1033.

Coolen, L.M., Wood, R.I., 1998. Bidirectional connections of the medial amygdaloid nucleus in the Syrian hamster brain: simultaneous anterograde and retrograde tract tracing. J. Comp. Neurol. 399, 189–209.

Davidson, R.J., Irwin, W., 1999. The functional neuroanatomy of emotion and affective style. Trends Cogn. Sci. 3, 11–21.

Davis, M., Walker, D.L., Lee, Y., 1997. Amygdala and bed nucleus of the stria terminalis: differential roles in fear and anxiety measured with the acoustic startle reflex. Philos. Trans. Biol. Sci. 352, 1675–1687.

Decampo, D.M., Fudge, J.L., 2013. Amygdala projections to the lateral bed nucleus of the stria terminalis in the macaque: comparison with ventral striatal afferents. J. Comp. Neurol. 521, 3191–3216.

Desikan, R.S., Ségonne, F., Fischl, B., Quinn, B.T., Dickerson, B.C., Blacker, D., Buckner, R.L., Dale, A.M., Maguire, R.P., Hyman, B.T., Albert, M.S., Killiany, R.J., 2006. An automated labeling system for subdividing the human cerebral cortex on MRI scans into gyral based regions of interest. Neuroimage 31, 968–980.

Dong, H.-W., Swanson, L.W., 2004a. Organization of axonal projections from the anterolateral area of the bed nuclei of the stria terminalis. J. Comp. Neurol. 468, 277–298.

Dong, H.-W., Swanson, L.W., 2004b. Projections from bed nuclei of the stria terminalis, posterior division: implications for cerebral hemisphere regulation of defensive and reproductive behaviors. J. Comp. Neurol. 471, 396–433.

Dong, H.-W., Swanson, L.W., 2006a. Projections from bed nuclei of the stria terminalis, magnocellular nucleus: implications for cerebral hemisphere regulation of micturition, defecation, and penile erection. J. Comp. Neurol. 494, 108–141.

Dong, H.-W., Swanson, L.W., 2006b. Projections from bed nuclei of the stria terminalis, anteromedial area: cerebral hemisphere integration of neuroendocrine, autonomic, and behavioral aspects of energy balance. J. Comp. Neurol. 494, 142–178.

Dong, H.-W., Swanson, L.W., 2006c. Projections from bed nuclei of the stria terminalis, dorsomedial nucleus: implications for cerebral hemisphere integration of neuroendocrine, autonomic, and drinking responses. J. Comp. Neurol. 494, 75–107.

Dong, H.-W., Petrovich, G.D., Swanson, L.W., 2000. Organization of projections from the juxtacapsular nucleus of the BST: a PHAL study in the rat. Brain Res. 859, 1–14.

Dong, H.-W., Petrovich, G.D., Swanson, L.W., 2001a. Topography of projections from amygdala to bed nuclei of the stria terminalis. Brain Res. Rev. 38, 192–246.

Dong, H.-W., Petrovich, G.D., Watts, a G., Swanson, L.W., 2001b. Basic organization of projections from the oval and fusiform nuclei of the bed nuclei of the stria terminalis in adult rat brain. J. Comp. Neurol. 436, 430–455.

Dumont, E.C., Mark, G.P., Mader, S., Williams, J.T., 2005. Self-administration enhances excitatory synaptic transmission in the bed nucleus of the stria terminalis. Nat. Neurosci. 8, 413–414.

Etkin, A., 2010. Functional neuroanatomy of anxiety: a neural circuit perspective. In: Stein, M.B., Steckler, T. (Eds.), Behavioral Neurobiology of Anxiety and Its Treatment. Springer Berlin Heidelberg, Berlin, Heidelberg, pp. 251–277.

Etkin, A., Prater, K.E., Schatzberg, A.F., Menon, V., Greicius, M.D., 2009. Disrupted amygdalar subregion functional connectivity and evidence of a compensatory network in generalized anxiety disorder. Arch. Gen. Psychiatry 66, 1361–1372.

Fedorov, A., Beichel, R., Kalpathy-Cramer, J., Finet, J., Fillion-Robin, J.-C., Pujol, S., Bauer, C., Jennings, D., Fennessy, F., Sonka, M., Buatti, J., Aylward, S., Miller, J.V., Pieper, S., Kikinis, R., 2012. 3D Slicer as an image computing platform for the Quantitative Imaging Network. Magn. Reson. Imaging 30, 1323–1341.

First, M.B., Spitzer, R.L., Gibbon, M., Williams, J.B.W., 2002. Structured Clinical Interview For DSM-IV-TR Axis I Disorders, Research Version, Patient Edition (SCID-I/P). Biometrics Research, New York State Psychiatric Institute, New York.

Fox, A.S., Shelton, S.E., Oakes, T.R., Davidson, R.J., Kalin, N.H., 2008. Trait-like brain activity during adolescence predicts anxious temperament in primates. PLoS One 3, e2570.

Ghashghaei, H., Hilgetag, C.C., Barbas, H., 2007. Sequence of information processing for emotions based on the anatomic dialogue between prefrontal cortex and amygdala. Neuroimage 34, 905–923.

Goldstein, R.Z., Volkow, N.D., 2002. Drug addiction and its underlying neurobiological basis: neuroimaging evidence for the involvement of the frontal cortex. Am. J. Psychiatry 159, 1642–1652.

Good, P., 2000. Permutation Tests: a Practical Guide to Resampling Methods for Testing Hypotheses, 2nd ed. Springer, New York.

Gray, H., 1918. Anatomy of the Human Body.

Greicius, M.D., Supekar, K., Menon, V., Dougherty, R.F., 2009. Resting-state functional connectivity reflects structural connectivity in the default mode network. Cereb. Cortex 19, 72–78.

Grupe, D.W., Oathes, D.J., Nitschke, J.B., 2013. Dissecting the anticipation of aversion reveals dissociable neural networks. Cereb. Cortex 23, 1874–1883.

Hagmann, P., Cammoun, L., Gigandet, X., Meuli, R., Honey, C.J., Wedeen, V., Sporns, O., 2008. Mapping the structural core of human cerebral cortex. PLoS Biol. 6, 1479–1493.

Hammack, S.E., Richey, K.J., Watkins, L.R., Maier, S.F., 2004. Chemical lesion of the bed nucleus of the stria terminalis blocks the behavioral consequences of uncontrollable stress. Behav. Neurosci. 118, 443–448.

Hasler, G., Fromm, S., Alvarez, R.P., Luckenbaugh, D.A., Drevets, W.C., Grillon, C., 2007. Cerebral blood flow in immediate and sustained anxiety. J. Neurosci. 27, 6313–6319.

Hines, M., Davis, F.C., Coquelin, A., Goy, R.W., Gorski, R.A., 1985. Sexually dimorphic regions in the medial preoptic area and the bed nucleus of the stria terminalis of the guinea pig brain: a description and an investigation of their relationship to gonadal steroids in adulthood. J. Neurosci. 5, 40–47.

Hines, M., Allen, L.S., Gorski, R.A., 1992. Sex differences in subregions of the medial nucleus of the amygdala and the bed nucleus of the stria terminalis of the rat. Brain Res. 579, 321–326.

Honey, C.J., Sporns, O., Cammoun, L., Gigandet, X., Thiran, J.P., Meuli, R., Hagmann, P., 2009. Predicting human resting-state functional connectivity from structural connectivity. Proc. Natl. Acad. Sci. U. S. A. 106, 2035–2040.

Jennings, J.H., Sparta, D.R., Stamatakis, A.M., Ung, R.L., Pleil, K.E., Kash, T.L., Stuber, G.D., 2013. Distinct extended amygdala circuits for divergent motivational states. Nature 496, 224–228.

Kalin, N.H., Shelton, S.E., Fox, A.S., Oakes, T.R., Davidson, R.J., 2005. Brain regions associated with the expression and contextual regulation of anxiety in primates. Biol. Psychiatry 58, 796–804.

Kash, T.L., Matthews, R.T., Winder, D.G., 2008. Alcohol inhibits NR2B-containing NMDA receptors in the ventral bed nucleus of the stria terminalis. Neuropsychopharmacology 33, 1379–1390.

Kim, M.J., Loucks, R.A., Palmer, A.L., Brown, A.C., Solomon, K.M., Marchante, A.N., Whalen, P.J., 2011. The structural and functional connectivity of the amygdala: from normal emotion to pathological anxiety. Behav. Brain Res. 223, 403–410.

Kim, S.-Y., Adhikari, A., Lee, S.Y., Marshel, J.H., Kim, C.K., Mallory, C.S., Lo, M., Pak, S., Mattis, J., Lim, B.K., Malenka, R.C., Warden, M.R., Neve, R., Tye, K.M., Deisseroth, K., 2013. Diverging neural pathways assemble a behavioural state from separable features in anxiety. Nature 496, 219–223.

Koch, M.A., Norris, D.G., Hund-Georgiadis, M., 2002. An investigation of functional and anatomical connectivity using magnetic resonance imaging. Neuroimage 16, 241–250.

Koob, G.F., Le Moal, M., 2008. Neurobiological mechanisms for opponent motivational processes in addiction. Philos. Trans. R. Soc. B-Biol. Sci. 363, 3113–3123.

Koob, G.F., Volkow, N.D., 2010. Neurocircuitry of addiction. Neuropsychopharmacology 35, 217–238.

Leri, F., Flores, J., Rodaros, D., Stewart, J., 2002. Blockade of stress-induced but not cocaine-induced reinstatement by infusion of noradrenergic antagonists into the bed nucleus of the stria terminalis or the central nucleus of the amygdala. J. Neurosci. 22, 5713–5718.

Lesur, A., Gaspar, P., Alvarez, C., Berger, B., 1989. Chemoanatomic compartments in the human bed nucleus of the stria terminalis. Neuroscience 32, 181–194.

Lewinsohn, P.M., Gotlib, I.H., Lewinsohn, M., Seeley, J.R., Allen, N.B., 1998. Gender differences in anxiety disorders and anxiety symptoms in adolescents. J. Abnorm. Psychol. 107, 109–117.

Logothetis, N.K., Wandell, B. a, 2004. Interpreting the BOLD signal. Annu. Rev. Physiol. 66, 735–769.

Lombardo, M.V., Ashwin, E., Auyeung, B., Chakrabarti, B., Taylor, K., Hackett, G., Bullmore, E.T., Baron-Cohen, S., 2012. Fetal testosterone influences sexually dimorphic gray matter in the human brain. J. Neurosci. 32, 674–680.

Lungwitz, E.A., Molosh, A., Johnson, P.L., Harvey, B.P., Dirks, R.C., Dietrich, A., Minick, P., Shekhar, A., Truitt, W. a, 2012. Orexin-A induces anxiety-like behavior through interactions with glutamatergic receptors in the bed nucleus of the stria terminalis of rats. Physiol. Behav. 107, 726–732.

Mai, J.K., Paxinos, G., Voss, T., 2008. Atlas of the Human Brain, 3rd ed. Elsevier, New York.

McLean, C.P., Asnaani, A., Litz, B.T., Hofmann, S.G., 2011. Gender differences in anxiety disorders: prevalence, course of illness, comorbidity and burden of illness. J. Psychiatr. Res. 45, 1027–1035.

Mishra, A., Rogers, B.P., Chen, L.M., Gore, J.C., 2013. Functional connectivity-based parcellation of amygdala using self-organized mapping: A data driven approach. Hum. Brain Mapp. http://dx.doi.org/10.1002/hbm.22249.

Murphy, K., Birn, R.M., Handwerker, D.A., Jones, T.B., Bandettini, P.A., 2009. The impact of global signal regression on resting state correlations: are anti-correlated networks introduced? Neuroimage 44, 893–905.

O'Daly, O.G., Trick, L., Scaife, J., Marshall, J., Ball, D., Phillips, M.L., Williams, S.S.C., Stephens, D.N., Duka, T., 2012. Withdrawal-associated increases and decreases in functional neural connectivity associated with altered emotional regulation in alcoholism. Neuropsychopharmacology 37, 2267–2276.

Oler, J.A., Birn, R.M., Patriat, R., Fox, A.S., Shelton, S.E., Burghy, C.A., Stodola, D.E., Essex, M.J., Davidson, R.J., Kalin, N.H., 2012. Evidence for coordinated functional activity within the extended amygdala of non-human and human primates. Neuroimage 61, 1059–1066.

Olson, I.R., Plotzker, A., Ezzyat, Y., 2007. The enigmatic temporal pole: a review of findings on social and emotional processing. Brain 130, 1718–1731.

Polston, E.K., Gu, G., Simerly, R.B., 2004. Neurons in the principal nucleus of the bed nuclei of the stria terminalis provide a sexually dimorphic GABAergic input to the anteroventral periventricular nucleus of the hypothalamus. Neuroscience 123, 793–803.

Price, J.L., Amaral, D.G., 1981. An autoradiographic study of the projections of the central nucleus of the monkey amygdala. J. Neurosci. 1, 1242–1259.

R Core Development Team, 2008. R: a Language and Environment for Statistical Computing. R Foundation for Statistical Computing, Vienna, Austria.

Reynolds, S.M., Zahm, D.S., 2005. Specificity in the projections of prefrontal and insular cortex to ventral striatopallidum and the extended amygdala. J. Neurosci. 25, 11757–11767.

Roy, A.K., Shehzad, Z., Margulies, D.S., Kelly, a M.C., Uddin, L.Q., Gotimer, K., Biswal, B.B., Castellanos, F.X.X., Milham, M.P., 2009. Functional connectivity of the human amygdala using resting state fMRI. Neuroimage 45, 614–626.

Saad, Z.S., Gotts, S.J., Murphy, K., Chen, G., Jo, H.J., Martin, A., Cox, R., 2012. Trouble at rest: how correlation patterns and group differences become distorted after global signal regression. Brain Connect. 2, 25–32.

Shin, L.M., Liberzon, I., 2010. The neurocircuitry of fear, stress, and anxiety disorders. Neuropsychopharmacology 35, 169–191.

Silberman, Y., Winder, D.G., 2013. Emerging role for corticotropin releasing factor signaling in the bed nucleus of the stria terminalis at the intersection of stress and reward. Front. Psychiatry 4, 42.

Smith, S.M., 2002. Fast robust automated brain extraction. Hum. Brain Mapp. 17, 143–155.

Somerville, L.H., Whalen, P.J., Kelley, W.M., 2010. Human bed nucleus of the stria terminalis indexes hypervigilant threat monitoring. Biol. Psychiatry 68, 416–424.

Somerville, L.H., Wagner, D.D., Wig, G.S., Moran, J.M., Whalen, P.J., Kelley, W.M., 2013. Interactions between transient and sustained neural signals support the generation and regulation of anxious emotion. Cereb. Cortex 23, 49–60.

Sullivan, G.M., Apergis, J., Bush, D.E.A., Johnson, L.R., Hou, M., Ledoux, J.E., 2004. Lesions in the bed nucleus of the stria terminalis disrupt corticosterone and freezing responses elicited by a contextual but not by a specific cue-conditioned fear stimulus. Neuroscience 128, 7–14.

Sun, N., Roberts, L, Cassell, M.D., 1991. Rat central amygdaloid nucleus projections to the bed nucleus of the stria terminalis. Brain Res. Bull. 27, 651–662.

Van den Heuvel, M.P., Mandl, R.C.W., Kahn, R.S., Hulshoff Pol, H.E., 2009. Functionally linked resting-state networks reflect the underlying structural connectivity architecture of the human brain. Hum. Brain Mapp. 30, 3127–3141.

Waddell, J., Morris, R., Bouton, M., 2006. Effects of bed nucleus of the stria terminalis lesions on conditioned anxiety: aversive conditioning with long-duration conditional stimuli and reinstatement of extinguished fear. Behav. Neurosci. 120, 324–336.

Whitfield-Gabrieli, S., Nieto-Castanon, A., 2012. Conn: a functional connectivity toolbox for correlated and anticorrelated brain networks. Brain Connect. 2, 125–141.

Wood, R.I., Swann, J.M., 2005. The bed nucleus of the stria terminalis in the Syrian hamster: subnuclei and connections of the posterior division. Neuroscience 135, 155–179.

Woodward, N.D., Karbasforoushan, H., Heckers, S., 2012. Thalamocortical dysconnectivity in schizophrenia. Am. J. Psychiatry 169, 1092–1099.